



Automated Water Extraction Index: A new technique for surface water mapping using Landsat imagery



Gudina L. Feyisa^{a,*}, Henrik Meilby^a, Rasmus Fensholt^b, Simon R. Proud^b

^a Department of Food and Resource Economics, University of Copenhagen, Rolighedsvej 23, DK-1958 Frederiksberg C, Denmark

^b Department of Geosciences and Natural Resource Management, University of Copenhagen, Øster Voldgade 10, DK-1350 Copenhagen K, Denmark

ARTICLE INFO

Article history:

Received 16 April 2013

Received in revised form 3 August 2013

Accepted 21 August 2013

Available online 17 September 2013

Keywords:

Classification accuracy

Threshold stability

Subpixel

Mixed pixel

ABSTRACT

Classifying surface cover types and analyzing changes are among the most common applications of remote sensing. One of the most basic classification tasks is to distinguish water bodies from dry land surfaces. Landsat imagery is among the most widely used sources of data in remote sensing of water resources; and although several techniques of surface water extraction using Landsat data are described in the literature, their application is constrained by low accuracy in various situations. Besides, with the use of techniques such as single band thresholding and two-band indices, identifying an appropriate threshold yielding the highest possible accuracy is a challenging and time consuming task, as threshold values vary with location and time of image acquisition. The purpose of this study was therefore to devise an index that consistently improves water extraction accuracy in the presence of various sorts of environmental noise and at the same time offers a stable threshold value. Thus we introduced a new Automated Water Extraction Index (AWEI) improving classification accuracy in areas that include shadow and dark surfaces that other classification methods often fail to classify correctly. We tested the accuracy and robustness of the new method using Landsat 5 TM images of several water bodies in Denmark, Switzerland, Ethiopia, South Africa and New Zealand. Kappa coefficient, omission and commission errors were calculated to evaluate accuracies. The performance of the classifier was compared with that of the Modified Normalized Difference Water Index (MNDWI) and Maximum Likelihood (ML) classifiers. In four out of five test sites, classification accuracy of AWEI was significantly higher than that of MNDWI and ML (P -value < 0.01). AWEI improved accuracy by lessening commission and omission errors by 50% compared to those resulting from MNDWI and about 25% compared to ML classifiers. Besides, the new method was shown to have a fairly stable optimal threshold value. Therefore, AWEI can be used for extracting water with high accuracy, especially in mountainous areas where deep shadow caused by the terrain is an important source of classification error.

© 2013 Elsevier Inc. All rights reserved.

1. Introduction

Environmental changes and their impacts on natural systems and human societies are topics of research in a wide range of scientific fields. Surface water is among the most vital earth resources undergoing changes in time and space as a consequence of land use/cover (LULC) changes, climate change and other forms of environmental changes in many parts of the world. The ecological, social, health and economic effects of surface water changes have been the subject of academic study for many years (Alderman, Turner, & Tong, 2012; Bond, Lake, & Arthington, 2008; Charron et al., 2004; Kondo et al., 2002; Lake, 2003; Li, Wu, Dai, & Xu, 2012; Sun, Sun, Chen, and Gong (2012)). Changes in surface water may result in disasters such as flooding, outbreaks of waterborne disease and water shortage in dry tropical areas, which may involve loss of lives. Timely monitoring and delivery of data on

the dynamics of surface water are, therefore, essential for policy and decision making processes (Giardino, Bresciani, Villa, & Martinelli, 2010; Morss, Wilhelmi, Downton, & Grunfest, 2005).

Remote sensing has become an important source of information in analyzing and delivering data on changes in different earth resources, and surface water in particular. Examples of studies applying remote sensing and GIS techniques for various applications in relation to water resources include flood hazard/damage assessment and management (Dewan, Islam, Kumamoto, & Nishigaki, 2007; Ji, Zhang, & Wylie, 2009; Proud, Fensholt, Rasmussen, & Sandholt, 2011), change in surface water resources (Gardelle, Hiernaux, Kergoat, & Grippa, 2009; Haas, Bartholomé, & Combal, 2009; Prigent et al., 2012), water quality assessment and monitoring (Guttler, Niculescu, & Gohin, 2013; He et al., 2012; Novoa et al., 2012), and water-related disease epidemiology (Charoenpanyanet & Chen, 2008; Dambach et al., 2012; Lacaux, Tourre, Vignolles, Ndione, & Lafaye, 2007).

Satellite sensors of varying spatial, temporal and spectral resolution have been used to extract and analyze information regarding surface water. Landsat satellites are among the most widely used optical

* Corresponding author. Tel.: +45 91414185; fax: +45 353 31508.

E-mail addresses: fgudina@gmail.com, fgudina@ifro.ku.dk (G.L. Feyisa), heme@ifro.ku.dk (H. Meilby), rf@geo.ku.dk (R. Fensholt), srp@geo.ku.dk (S.R. Proud).

sensors in surface water and other environmental research. The use of these remotely sensed data commonly starts with classification of land use/cover types. Common water classification methods for optical imagery could be categorized into four basic types (Ji et al., 2009): (a) thematic classification (Lira, 2006), (b) linear unmixing (Sethre, Rundquist, & Todhunter, 2005), (c) single-band thresholding (Jain, Singh, Jain, & Lohani, 2005) and (d) two-band spectral water indices (Jain, Saraf, Goswami, & Ahmad, 2006; McFeeters, 1996; Rogers & Kearney, 2004; Xu, 2006). Combinations of various methods are also proposed to improve water extraction accuracies. Examples are, Jiang, Qi, Su, Zhang, and Wu (2012), Sheng, Shah, and Smith (2008), Sun et al. (2012) and Verpoorter, Kutser, and Tranvik (2012). Single band thresholding and two-band indices are commonly used water extraction methods because of ease of use and the fact that these methods are computationally less time-consuming than alternative approaches (Ryu, Won, & Min, 2002).

McFeeters (1996) introduced the Normalized Difference Water Index (NDWI) to delineate open water features using the *green* (band 2) and *near-infrared* (band 4) of Landsat TM. Rogers and Kearney (2004) used another NDWI for water extraction where they applied bands 3 and 5 of Landsat TM. McFeeters (1996) proposed a threshold of 0 for extracting surface water using the raw digital number of Landsat, where all positive NDWI values would be classified as water and negative values as nonwater. However, Xu (2006) found that the NDWI cannot efficiently suppress the signal from built-up surfaces and using an NDWI threshold of 0 does not accurately enable discriminating built-up surfaces from water pixels. Xu (2006) therefore proposed another index, called Modified Normalized Difference Water Index (MNDWI), where McFeeters (1996) NDWI was modified by replacing band 4 by band 5 of Landsat 5 TM. The MNDWI of Xu (2006) is one of the most widely used water indices for various applications, including surface water mapping, land use/cover change analyses and ecological research (Davranche, Lefebvre, & Poulin, 2010; Duan & Bastiaansen, 2013; Hui, Xu, Huang, Yu, & Gong, 2008; Poulin, Davranche, & Lefebvre, 2010).

Even though a number of water extraction techniques are described in the literature, the choice between them is constrained by accuracy problems. Environmental monitoring and change detection techniques such as post-classification comparison are likely to be less reliable when classifiers of low accuracy are used (Congalton & Green, 2009; Mucher, Steinnocher, Kressler, & Heunks, 2000). For instance, in a study focusing on water dynamics monitoring, Ji et al. (2009) faced two major problems in appropriately using water indices: first, the results obtained using different indices were inconsistent and unreliable; second, the threshold values applied to distinguish water from non-water were unstable, varying with scene and locations. These authors compared four different water indices using simulated datasets of four satellite sensors: Landsat ETM+, Système Pour l'Observation de la Terre (SPOT), the Advanced Space-borne Thermal Emission and Reflection radiometer (ASTER), and the Moderate Resolution Imaging Spectroradiometer (MODIS), aiming to identify the best method for delineating water features. Among the four alternatives, they found that the MNDWI performed best in delineating water, and featured the most stable threshold.

Water classification accuracy problems may be especially pronounced in areas where the background land cover includes low albedo surfaces such as asphalt roads in urban areas, and shadows from mountains, buildings and clouds. The presence of shadows may cause misclassification due to the similarity in reflectance patterns, and this may lessen the accuracy of surface water mapping and change analysis (Frey, Huggel, Paul, & Haeblerli, 2010; Verpoorter et al., 2012; Xu, 2006). In environments where nonwater dark surfaces are found, simple classification methods such as two-band water indices and single-band thresholding may not sufficiently and accurately distinguish between water pixels and nonwater dark surfaces, particularly shadows (Verpoorter et al., 2012). In a study of land cover dynamics using

Landsat TM data, we noted accuracy problems due to failure of existing water extraction methods in accurately distinguishing water from shadows and low albedo urban surfaces. Particularly, no existing water index was able to automatically separate water and shadowed surfaces. In this paper, therefore, we introduce a multiple-band index called Automated Water Extraction Index (AWEI), with the objectives to: (a) improve accuracy of surface water mapping by automatically suppressing classification noise from shadow and other nonwater dark surfaces, and (b) test the robustness of the new method under different environmental conditions and evaluate its relative accuracy in comparison with existing classification techniques.

2. Study areas and data sources

2.1. Test sites

The accuracy and robustness of the Automated Water Extraction Index (AWEI) were tested considering several lakes and other water bodies in different environmental conditions ranging from humid temperate through sub-tropical to tropical dry regions. The test water bodies were obtained from five different countries: Denmark, Switzerland, Ethiopia, South Africa and New Zealand. The water bodies that include small freshwater reservoirs, large lakes, harbors and the sea differ with regard to depth, turbidity, chemical composition and surface appearance. A summary of the basic characteristics of the test sites is shown in Table 1.

The test sites were deliberately selected so that the sub-scenes consist of complex surface features, such as hill shade, built-up areas and other dark surfaces as background to the water bodies. The test sites in Switzerland, Ethiopia and South Africa are characterized by the presence of built-up surfaces and shadows of mountains. The site in Denmark also consists primarily of urban background but with no major shadow problems since the terrain is predominantly flat and tall buildings in the urban area are rare. The test site in New Zealand consists of mountain slopes with deep shadows, but no major urban surfaces are included.

In addition to the five test sites for which detailed accuracy analyses and comparisons were carried out, further validation of the robustness of the new index was undertaken considering shadow-dominated water bodies in Norway, rivers with urban surfaces and shadows from tall buildings in Shanghai, China, and several crater lakes with built-up background surfaces in Bishoftu, Ethiopia. However, these additional test sites were not analyzed in detail and classification output from these sites is not included in the Results section; instead, the classification maps are included in Appendix A for visual inspection of classification accuracy.

2.2. Landsat images

Landsat 5 TM images were acquired from USGS GLOVIS portal (United States Geological Survey (USGS), 2012). All Landsat images used are of product type L1T and with a scene quality score of 9, which means perfect scenes with no errors detected. The images were also georeferenced with precision better than 0.4 pixels (NASA, 2012). The sub-scenes were all free of clouds. Descriptions of the Landsat images are presented in Table 2.

2.3. Reference data

Reference data used in accuracy assessment are described in Table 2. For the test site in Denmark, colored Digital Orthophoto Quadrangles (DOQs) from year 2010 were used as reference. These aerial photos have a spatial resolution of 12.5 cm and location accuracy better than 0.5 m (COWI, 2010). For the four other test sites, high spatial resolution images provided by Google Earth™ were used for reference. The acquisition dates of the reference data and the Landsat 5 TM images were

Table 1

Characteristics of the study sites.

The source of climate information is: (<http://www.climatedata.eu/>).

Country and name of water bodies	Center point coordinate (UTM)	Area (ha)	General characteristics of water bodies	Mean alt. (m)	Topography	Climate
Denmark Several artificial lakes, a harbor and the sea (Øresund and Køge Bugt)	6,172,085 m N, 12°34'57.42"E	2085	Shallow clear artificial lakes, clear seas	9	Predominantly flat	Temperate
Switzerland Lake Lauerz	5,209,030 m N, 469,608 m E	289	Clear lake	1100	Mountainous	Temperate
Ågeri lake	5,218,774 m N, 471,530 m E	719	Clear lake			
Sihl lake	5,218,191 m N, 484,028 m E	1034	Clear lake			
Wägitaler lake	5,214,616 m N, 494,092 m E	402	Clear lake			
Klöntaler lake	5,207,839 m N, 498,040 m E	309	Clear lake			
Ethiopia Gefersa	1,002,432 m N, 459,709 m E	144	Clear reservoir	2377	Mountainous	Tropical dry
Dire	1,011,794 m N, 493,000 m E	106	Turbid reservoirs			
Legedadi	1,002,374 m N, 497,446 m E	423	Turbid reservoirs			
South Africa Berg river	6,244,161 m S, 320,605 m E	426	Clear reservoir	600	Rugged hilly	Subtropical semi-arid
Wemmershoek	6,255,473 m S, 323,355 m E	195	Clear reservoir			
Brandvlei	6,265,857 m S, 354,413 m E	3097	Clear reservoir			
New Zealand Lake Te Anau	5,004,239 m S, 723,800 m E	6495	Large clear lake	800	Rugged hilly	Humid temperate

closely matched to minimize bias in the surface water boundaries that could arise because of large differences in time. The dates of acquisition of the Landsat images and reference data are shown in Table 2.

The “true” boundaries of all the test water bodies were digitized manually on-screen from the reference data. In the analysis, the manually digitized water map was used to assess the accuracy of the different water extraction methods when applied to the Landsat images.

3. Methods

3.1. Image preprocessing

Landsat 5 TM images acquired in the form of raw digital number were calibrated to surface reflectance values. Atmospheric correction was applied to all images using the Fast Line-of-Sight Atmospheric Analysis of Spectral Hypercubes (FLAASH) module in ENVI v. 4.8 (Exelis Visual Information Solutions, 2010). Aerosol Optical Depth (AOD) and total Column Water Vapor data to be used in the FLAASH atmospheric correction module were retrieved from MODIS Terra atmospheric products (Jimenez-Munoz, Sobrino, Mattar, & Franch, 2010) for each of the five test sites. The MODIS Terra products that had been acquired on the same date as the Landsat images were used to retrieve the calibration constants. Initial visibility was estimated using the aerosol optical thickness obtained from MODIS data using Eq. (1), where, VIS = initial visibility, Z = mixing layer height and AOD = Aerosol Optical Depth. The mixing layer height values for the test sites were not available. Therefore, a daytime mixing layer height of 1.5 km was used for all test sites (typical values range from 1 to 2 km (Butcher, Charlson,

Orians, & Wolfe, 1992)). Water vapor calibration constants for each of the Landsat images are summarized in Table 3. The overpass time of Landsat TM and MODIS Terra at each test site was closely matched (less than 2 h difference).

$$VIS = \frac{3.912}{AOD} * Z. \quad (1)$$

Image-to-image co-registration between the reference data and Landsat images was undertaken for the test sites in Denmark and Ethiopia. Manual co-registration was performed with a Root Mean Square Error (RMSE) of less than 0.4 pixels. At least 25 control points were used for co-registration of each image with the reference data. The co-registration between Landsat and Google Earth™ images at the rest of the test sites was already highly accurate and hence there was no need for manual co-registration. Since the L1T Landsat TM and ETM+ products are geometrically corrected (NASA, 2012), no such corrections were applied in the pre-processing.

3.2. Pure-pixel selection

An independent set of “pure” pixel reflectance values of nine major land cover types was sampled from the six reflective bands of a Landsat 5 TM image of Addis Ababa, acquired on Dec. 9, 2010. The land cover types are: water, vegetation (forest and non-forest), bright soil, dark soil, brown soil, bright built, asphalt, other dark built and shadow. Spectral data from these pure pixels were used to examine reflectance patterns and identify land cover types that affect water extraction accuracy, aiming to design a method that accurately discriminates between

Table 2

Description of Landsat TM scenes and corresponding reference data.

Test site	Landsat scene			Reference data and sources
	Acquisition date	Path	Row	
Water bodies in Copenhagen, Denmark	June 29, 2010	195	21	Colored Digital Orthophoto quadrangles acquired between May and July 2010, ©COWI
Lakes in Switzerland	Sept 30, 2009	195	27	Google Earth™ image acquired on Jul 1 2009
Reservoirs in Addis Ababa, Ethiopia	Dec 9, 2010	168	54	Google Earth™ image acquired on Oct 13 and Dec 20, 2010, ©Digital globe, CNES/SPOT Image
Reservoirs in South Africa	Mar 29, 2010	175	83	Google Earth™ image acquired on Jan 4, Jan 7 and Jan 18, 2010, ©GeoEye and AfriGIS
A lake in New Zealand	Feb 3, 2010	76	91	Google Earth™ image acquired on Apr 09, 2010 and Feb 16, 2011, ©GeoEye

Table 3
Calibration values used in atmospheric correction using FLAASH.

Test Site	Date of Landsat/MODIS Terra overpass	Average water vapor column from MODIS (g/cm ²)	Water vapor multiplier	Average aerosol optical thick-from MODIS	Visibility (km)
Denmark	Jun 29, 2010	3.00	1.03	0.33	17.8
Switzerland	Sept 30, 2009	1.43	0.49	0.08	73.4
Ethiopia	Dec 9, 2010	2.30	0.56	0.10	58.7
South Africa	Mar 29, 2010	1.90	0.46	0.033	177.8
New Zealand	Feb 3, 2010	2.67	0.91	0.12	48.9

such surfaces and water. The pure pixel data were intended neither for classification nor accuracy assessment and therefore, only the image of Addis Ababa and its surroundings was used for pure pixel extraction. The reason for choosing Addis Ababa for pure pixel extraction was that this area includes all the major challenging features influencing water extraction accuracy: shadow, dark built-up surfaces and other low albedo surfaces such as black soil.

The methods used to extract pure pixels of the selected land cover types include spectral feature space scatter plot from Minimum Noise Fraction Transform (MNFT) images, Pixel Purity Index (PPI), manual digitization from images accessed through Google Earth™, ground-based land cover assessment and the familiarity of the first author with the local area. Pure pixel samples for water were taken from the middle of lakes to avoid mixed edge pixels. Similarly, high forest with closed canopy from Menagesha national forest was applied for sampling vegetation pure pixels. Pure pixels of built-up land cover were sampled from homogenous surfaces such as airport runways and large warehouse roofs in Addis Ababa city. Since land cover types in Addis Ababa are highly heterogeneous, detection of pure built pixels was assisted by PPI and spectral feature space in ENVI v.4.8 (Exelis Visual Information Solutions, 2010). Shadow pixels were extracted by thresholding hill-shade images derived from elevation data using the ASTER Digital Elevation Model (DEM) in mountainous parts of the test site. Homogenous agricultural fields with exposed black, brown and bright soils were also sampled from the outskirts of the city.

For each land cover type, 312 pure pixels were extracted from the six reflective bands of the Landsat 5 TM images. Average reflectance values of the pure pixels are shown in Fig. 1. Separability of the spectral signatures of the selected nine major land cover types was tested by Jeffries–Matusita’s pairwise separability measure (Richards, 1993) in ENVI v. 4.8. All pairs of land cover types were found to be separable with values ranging from 1.89 to 2.0.

3.3. Formulation of the Automated Water Extraction Index (AWEI)

Five spectral bands of Landsat 5 TM were used in developing the new index (AWEI) to increase the contrast between water and other dark surfaces. The primary aim of the formulation of AWEI was to maximize separability of water and nonwater pixels through band differencing, addition and applying different coefficients. Accordingly, two separate equations are proposed to effectively suppress nonwater pixels and extract surface water with improved accuracy (Eqs. (2) and (3)). The coefficients used in Eqs. (2) and (3) and the arithmetic combinations of the chosen spectral bands were determined based on combinatorial examination of the reflectance properties of various land cover types. The coefficients of these equations are empirical results determined based on reflectance patterns observed across the dataset of pure pixels of various land cover types. An iterative process was applied to identify parameters that maximize the separability of water and nonwater surfaces characterized by low reflectance. In the final index, the coefficients were rounded for ease of use. Particular emphasis was given to the enhancement of the separability of water and dark surfaces such as shadow and built-up structures that are often difficult to distinguish due to

similarities in reflectance patterns. In addition to enhancing separability of water and nonwater pixels, the choice of the coefficients also aimed to stabilize the threshold needed to distinguish water from nonwater pixels by forcing nonwater pixels below 0 and water pixels above 0, implying that 0 could be used as a reasonable starting threshold for classifying land cover into binary classes of water and nonwater under a wide range of environmental conditions.

$$AWEI_{nsh} = 4 \times (\rho_{band2} - \rho_{band5}) - (0.25 \times \rho_{band4} + 2.75 \times \rho_{band7}) \quad (2)$$

$$AWEI_{sh} = \rho_{band1} + 2.5 \times \rho_{band2} - 1.5 \times (\rho_{band4} + \rho_{band5}) - 0.25 \times \rho_{band7} \quad (3)$$

where ρ is the reflectance value of spectral bands of Landsat 5 TM: band 1 (blue), band 2 (green), band 4 (NIR), band 5 (SWIR) and band 7 (SWIR).

$AWEI_{nsh}$ is an index formulated to effectively eliminate nonwater pixels, including dark built surfaces in areas with urban background and $AWEI_{sh}$ is primarily formulated for further improvement of accuracy by removing shadow pixels that $AWEI_{nsh}$ may not effectively eliminate. The subscript “nsh” in Eq. (2) is included to specify that the index is suited for situations where shadows are not a major problem. The subscript “sh” in Eq. (3) indicates that the equation is intended to effectively eliminate shadow pixels and improve water extraction accuracy in areas with shadow and/or other dark surfaces. But in areas with highly reflective surfaces such as ice, snow and reflective roofs in urban areas, Eq. (3) may misclassify such surfaces as water.

In Eq. (2), quadrupling the difference between the band 2 and band 5 results in large positive values for water pixels and negative values for most nonwater pixels. To help in discriminating water from other surfaces that have similar spectral patterns, band 4 and band 7 are subtracted from the result and different weights are assigned to these bands to force nonwater pixels to have even larger negative values; this subtraction will not to any greater extent lead to negative values for water pixels because water has very low reflectance in the spectral ranges of band 4 and band 7. The equation results in large negative values for pixels covered by vegetation, soil, bright built and other surfaces that have large reflectance for band 4 or 7. The equation is also intended to enhance separability between water, dark surfaces and other nonwater surfaces. In many cases, water absorbs almost all of the incoming radiation in bands 4, 5 and 7 and achieves relatively highest reflectance between bands 1 and 2 of Landsat 5 TM (Lillesand, Kiefer, & Chipman, 2004). Shadowed surfaces also have low reflectance in all spectral bands, but the magnitude of reflectance varies due to variation in surface characteristics and the depth of shadow. Hence, Eq. (2) alone may not completely eliminate all types of shadows and other low albedo surfaces. As shown in Fig. 1, for instance, subtracting band 5 from band 2 could yield positive values for both water and shadows. Quadrupling the difference and subtracting bands 4 and 7 may result in some shadow pixels obtaining similar values as that of water due to the similarity in reflectance patterns within these bands, hence making it difficult to exclude shadow pixels from water class.

Due to these limitations of Eq. (2), Eq. (3) was formulated to achieve enhanced separability of water and shadows and/or dark surfaces. It can

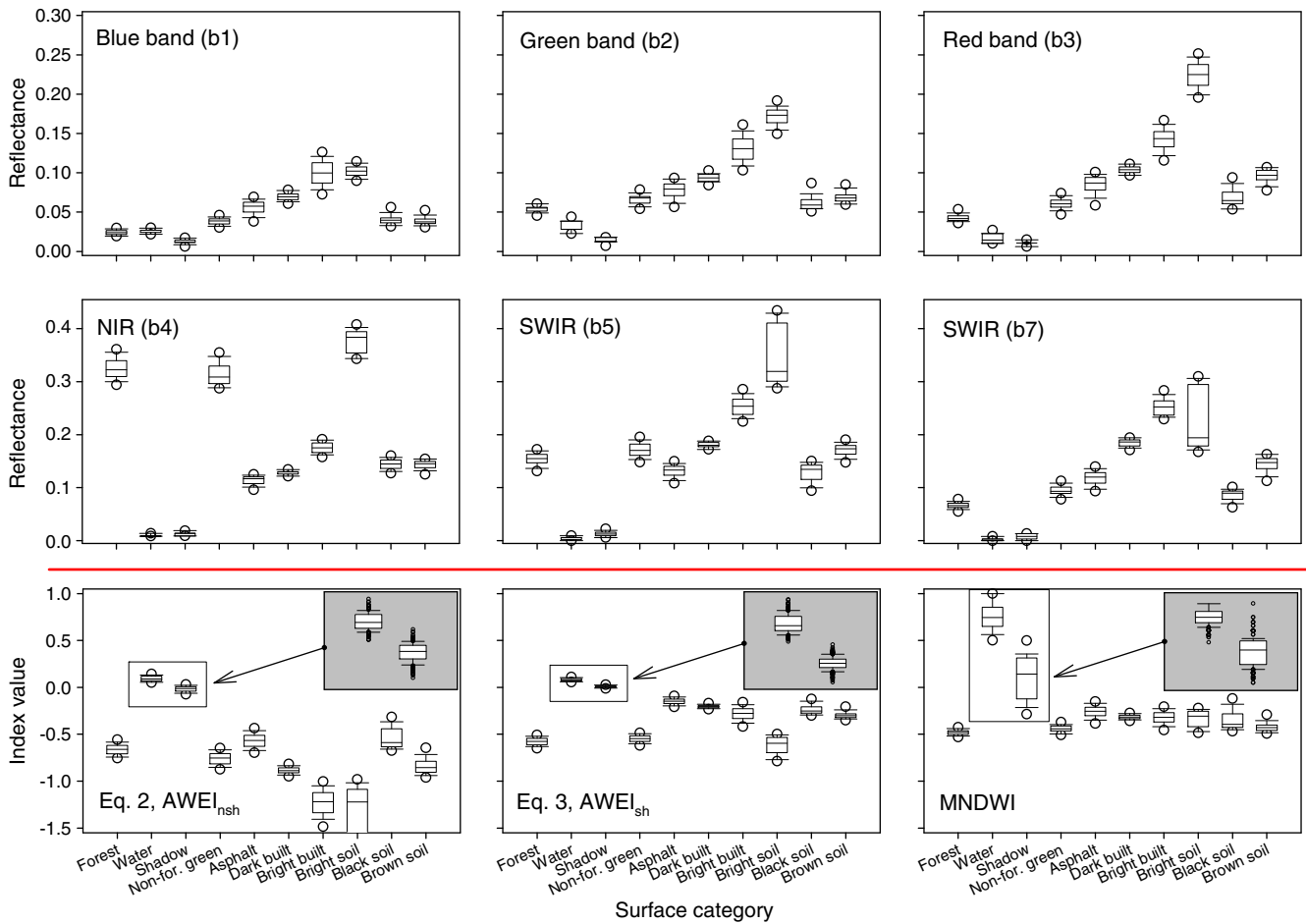


Fig. 1. Reflectance distributions of pure pixels of major land cover types. Each box plots shows the location of the 10th, 25th, 50th, 75th, and 90th percentiles using horizontal lines (boxes and whiskers) and the circles are 5th and 95th percentiles.

be noted from Fig. 1 that the largest difference between the reflectance of water and shadow is found in bands 1 and 2. Therefore, adding these two bands, while at the same time multiplying band 2 by the specified coefficient, enhances the separability between water and shadow pixels, yielding relatively large positive values for water pixels compared to shadow pixels. Subtracting bands 4, 5 and 7 forces nonwater pixels in the negative direction, and the net effect of this subtraction on water pixels is minimal compared to nonwater surfaces including shadows, which are forced considerably below zero. Band 3 was not used in Eqs. (2) and (3) because during the preliminary tests, including this band did not improve separability and accuracy. From the arithmetic formulation of Eq. (3), it may be noted that the addition of the short wave bands (bands 1 and 2) may result in large positive values for high albedo surfaces such as ice, cloud, and highly reflective building roofs. Eq. (3) may therefore not be able to distinguish these high-albedo surfaces from water.

Therefore, the intended use of the two AWEI equations is as follows: 1) in situations where shadows are major sources of accuracy loss but surfaces such as snow, ice and high albedo built surfaces are not present, $AWEI_{sh}$ alone is proposed to automatically enhance the separability of pixels of water from nonwater (more importantly from shadow pixels) so that application of a threshold close to 0 is suitable for the extraction of surface water; 2) in areas where shadows are not a major problem, $AWEI_{nsh}$ alone is proposed; 3) in conditions where both high albedo surfaces and shadow/dark surfaces are found, we propose using Eqs. (2) and (3) sequentially in a classification tree; 4) in areas with

no shadowed areas, no dark urban backgrounds and no high-albedo surfaces, either of the two can be used alone.

3.4. Classification, threshold optimization and per-pixel accuracy assessment

At the test sites in Denmark and Ethiopia, urban background dominates the sub-scenes. Therefore, both equations of AWEI ($AWEI_{nsh}$ and $AWEI_{sh}$) were applied sequentially: first, $AWEI_{nsh}$ was applied to the image; next, $AWEI_{sh}$ was used to eliminate misclassified pixels with shadows and other dark surfaces. At the test sites in Switzerland, New Zealand and South Africa, only $AWEI_{sh}$ was applied because urban surfaces are rare in these sites.

To compare accuracy of the proposed water extraction technique with other methods, we made preliminary tests of various water indices including the Water Index (WI) of Ouma and Tateishi (2006), the Normalized Difference Water Index (NDWI) of McFeeters (1996) and other indices that Ji et al. (2009) used in their studies. Based on this preliminary evaluation, it appeared that all indices, except the MNDWI, performed poorly at our test sites. We therefore only considered MNDWI for comparison with the new index proposed in this paper. A supervised maximum likelihood (ML) classifier was also included in our comparison as this classifier is one of the most widely used methods in land cover classification. For the ML classifier, water and nonwater training data were produced for each test site. The minimum size of reference datasets for training was determined using the multinomial conservative sample size equation described in Congalton and Green (2009). The

reference data were generated by digitizing multiple polygons on the true-color composites of Landsat bands and evenly distributing the samples across all parts of the sub-scenes. It was easy to generate large reference data units since the classes considered are only water and nonwater and it is relatively easy to visually distinguish between water and nonwater surfaces from high spatial resolution images retrieved through Google Earth™. These images were used to differentiate nonwater dark areas from water surfaces. No separate validation data were necessary for accuracy assessment of the ML classifier since the classification result was compared against the true map of water.

Since the AWEI equations are formulated to enhance separability of water and nonwater pixels by applying coefficients that force nonwater pixels below 0 and water pixels above 0, a threshold of 0 can be used as a default starting point. But due to variation in scene brightness and contrast with time and space, the default threshold may not always result in the highest possible water extraction accuracy that can be achieved by application of the index. In order to determine the optimal threshold, multiple thresholds were considered, and for each threshold value corresponding commission errors (over-estimation) and omission errors (under-estimation) were calculated and the percentage errors were plotted against threshold values. The intersection point of commission and omission error graphs was then considered as the optimal threshold since it approximates the minimum possible sum of the two error types. We evaluated the stability of optimal thresholds of the new method and of MNDWI by examining the variation of the optimal threshold values for the two indices across the five test sites.

Classification accuracy of the three methods, i.e. AWEI, MNDWI and ML, was assessed by calculating kappa coefficients and error matrices. The accuracy comparison between AWEI and MNDWI was made at their optimal thresholds. McNemar's statistical test was applied to examine whether the new water extraction method significantly improves accuracy compared to MNDWI and ML in the test sites. McNemar's continuity corrected chi-square statistic was computed as shown in Eq. (4) (De Leeuw et al., 2006):

$$\chi^2 = \frac{(|f_{12} - f_{21}| - 1)^2}{f_{12} + f_{21}} \quad (4)$$

where, f_{12} and f_{21} denote the frequencies of cases that are correctly classified by one classification method but wrongly classified by the other.

3.5. Sub-pixel accuracy assessment

The sensitivity of different classifiers to various mixtures of water and nonwater was evaluated using sub-pixel commission–omission errors and by plotting graphs showing the cumulative percentage of edge pixels classified as water against the proportion of each individual pixel covered by water for mixed edge pixels at test sites in Denmark, Switzerland and Ethiopia. Detailed sub-pixel accuracy analysis and comparisons were undertaken using the three reservoirs in Ethiopia (Gefersa, Dire and Legedadi). The total number of mixed edge pixels in the three reservoirs was 1819 (164 ha). In the sub-pixel accuracy assessment, commission and omission errors brought about by edge pixels were quantified by the use of an overlay analysis in ArcGIS. Any pixels that included water and nonwater surfaces were considered to be mixed edge pixels (Fig. 2). If a mixed edge pixel was classified as water, the fraction of it that fell outside the “true” boundary was considered to be sub-pixel commission error. Similarly, in cases where mixed pixels are classified as nonwater, the fraction of these pixels that fell inside the “true” water body was considered to be an omission error at the sub-pixel level. Mixed pixels consisting predominantly of water (>50% water) should ideally be classified as water and vice versa. In the sub-pixel accuracy assessment, influences of misregistration artifacts and manual digitization of true water boundaries were assumed to be insignificant.

4. Results

4.1. Water extraction maps

The outputs of water extraction using the three classifiers at the five test sites are presented in Fig. 3. Visual inspection of Fig. 3 indicated that AWEI resulted in better accuracy of surface water mapping compared to MNDWI and ML. Particularly at test sites in Switzerland, South Africa and New Zealand, the new index (AWEI) was consistently better in suppressing shadow and other nonwater surfaces. In most cases, MNDWI

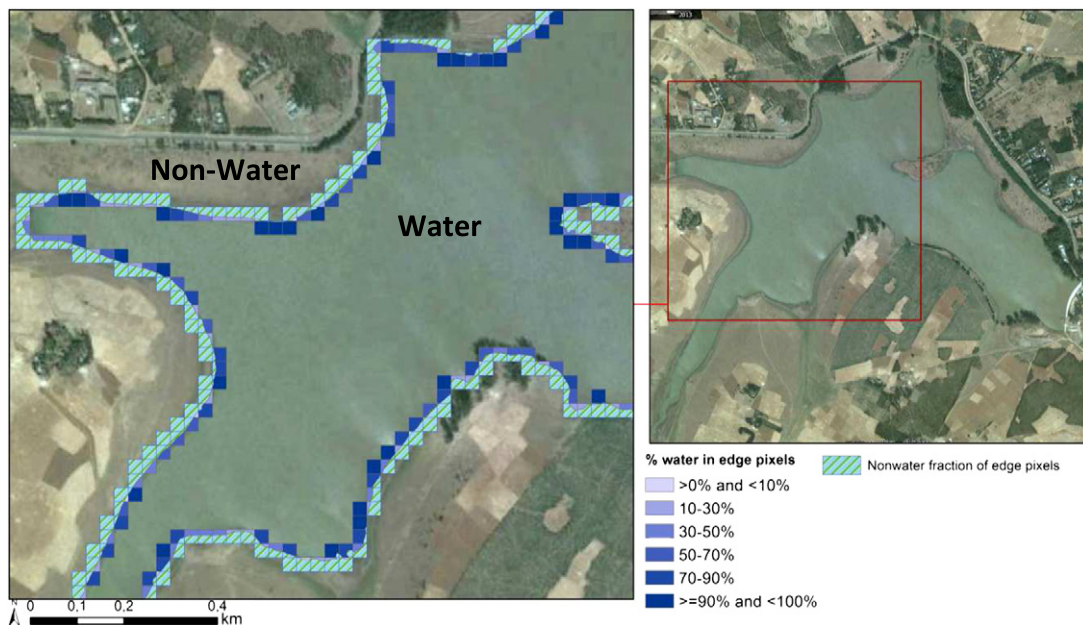


Fig. 2. Edge pixels around Gefersa reservoir (Ethiopia) showing mixed pixels with different proportions of water (shown on high spatial resolution image accessed through Google Earth™).

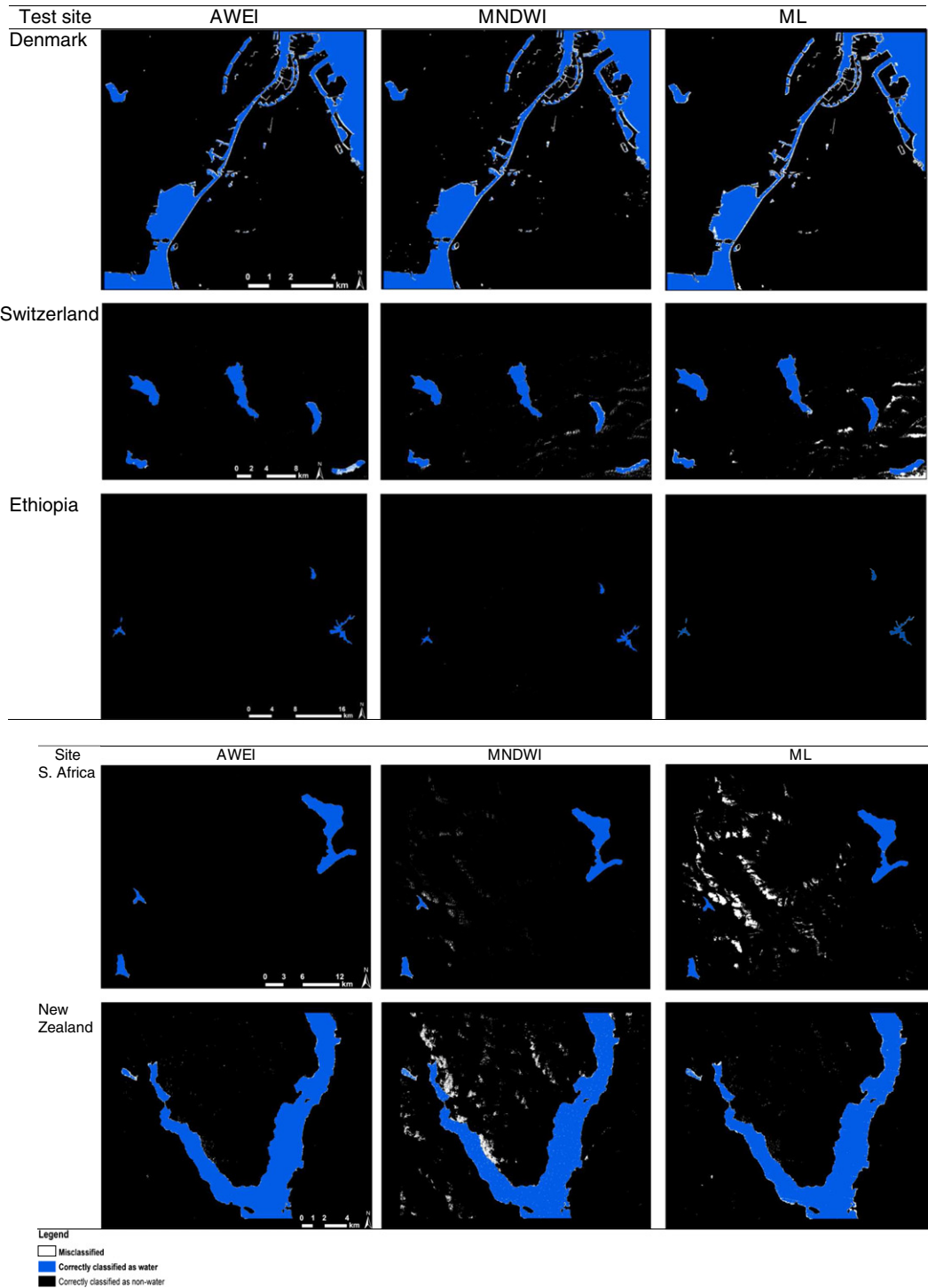


Fig. 3. Comparison of water extraction results using three classifiers at the five test sites.

and especially ML produced noisy results. However, at test sites in Denmark and Ethiopia, visual inspection of Fig. 3 indicated smallest difference among the three classification methods.

Visual inspection of classification outputs at the three additional test sites shown in Appendix A (Figs. A1–A3) also indicates that AWEI is effective in extracting surface water in the presence of shadow and urban surfaces. At Bishoftu lakes in Ethiopia, where no major shadow surfaces were present, both $AWEI_{sh}$ and MNDWI resulted in (visually) similar classification outputs. By contrast, at the test sites in Norway

and Shanghai where dark shadows were abundant, visual inspection clearly shows that $AWEI_{sh}$ suppressed shadowed surfaces more effectively than MNDWI (shown in Appendix A).

4.2. Classification accuracy and edge pixel effects

The results of mapping accuracy at each of the five main test sites are summarized in Table 4. At all test sites the accuracy achieved by AWEI was higher than that of the MNDWI and ML classifiers. Averaged over

Table 4
Summary of classification accuracy of the three classifiers by test site.

Classifier	Denmark	Switzerland	Ethiopia	S. Africa	New Zealand
	Kappa coeff.				
AWEI	0.93	0.95	0.97	0.98	0.98
MNDWI	0.92	0.89	0.95	0.94	0.90
ML	0.89	0.81	0.93	0.62	0.97

the five test sites the total omission and commission error of AWEI was only about 50% of that of the MNDWI and 25% of that of the ML classifiers (Fig. 4). Details of accuracy assessment including users' and producers' accuracy are shown in Appendix A (Table A1). Since visual inspection from Fig. 3 indicates small variation in accuracy at test sites in Denmark and Ethiopia, McNemar's chi-square test of significance of accuracy difference at the test sites in Denmark, Switzerland and Ethiopia are included in Table 5. At these three test sites, significant accuracy improvement was achieved by AWEI (P-value < 0.01) compared to ML. At the test site in Denmark, accuracy difference between AWEI and MNDWI was insignificant (Table 5). ML performed worst at test site in South Africa (kappa coefficient 0.62) and at this test site, the highest accuracy was achieved by AWEI, with a kappa coefficient of 0.98 (Table A1 in Appendix A).

The sub-pixel accuracy analysis is presented in Fig. 5. The comparison shows the ability of the three classifiers in correctly classifying edge pixels with various mixtures of water and nonwater components. The vertical line in Fig. 5 indicates the 50% water–nonwater mixture and the figure shows that among the edge pixels that AWEI classified as water, only 13% were predominantly nonwater. Conversely, 87% of mixed edge pixels that were classified as water were correctly classified by AWEI. Using MNDWI, 81% of the mixed edge pixels were correctly classified. Further analysis of mixed edge pixels at test sites in Addis Ababa showed that sub-pixel commission error of AWEI corresponded to an overestimation of 16.6 ha (total area of predominantly nonwater edge pixels classified as water), and omission error corresponded to 4.3 ha (total area of predominantly water edge pixels classified as nonwater). For comparison, edge pixel commission and omission errors of MNDWI corresponded to overestimation and underestimation of 18.3 ha and 4 ha, respectively. At this site edge pixel omission and commission error of ML corresponded to 49.3 ha and 0.6 ha, respectively.

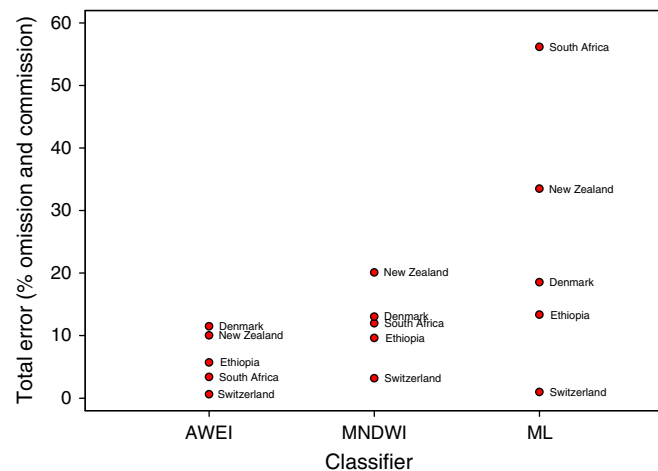


Fig. 4. Total classification error (combined commission and omission error). The box plots show the variability of classification errors among test sites. Each box plots shows the location of the 10th, 25th, 50th, 75th, and 90th percentiles using horizontal lines (boxes and whiskers) and the circles are 5th and 95th percentiles.

Table 5
Summary of McNemar's continuity corrected χ^2 test for differences in classification accuracy.

Test sites	Classifier	χ^2		P-value	
		MNDWI	ML	MNDWI	ML
Denmark	AWEI	0.8	114	0.30	0.00
Switzerland	AWEI	408.0	619	0.00	0.00
Ethiopia	AWEI	19.0	30	0.00	0.00

Based on the sum of total overestimation and underestimation of edge pixels, AWEI performed slightly better than MNDWI, and ML achieved the lowest accuracy in classifying mixed edge pixels.

4.3. Optimal threshold and its variability

A comparison of the stability of the optimum thresholds of AWEI and MNDWI is shown in Fig. 6. It clearly appears that the optimal threshold of MNDWI at different test sites exhibited large variation compared to AWEI. The optimal threshold of MNDWI ranged from 0.005 in Denmark to 0.6 in South Africa, whereas for AWEI the optimal threshold only varied from -0.15 ($AWEI_{lsh}$ in Denmark) to 0.045 ($AWEI_{sh}$ in South Africa), and in the three other sites the optimal threshold of $AWEI_{sh}$ was 0 (Fig. 6).

5. Discussion and perspectives

The new water extraction index introduced in this paper contributes to the efforts being made to improve the accuracy of surface water mapping and change analysis for various environmental studies and applications. This method uses a simple and systematic technique of enhancing class separability without a need for additional data to remove shadow and dark surface noises, which are often major causes of misclassification in surface water mapping. Using a simple classification tree approach, the AWEI was shown to extract surface water with high accuracy, particularly in mountainous areas where hills cast shadows on background surfaces and in urban areas with complex land cover. AWEI is not only a simple technique but was also shown to be robust under various environmental conditions and for different types of water bodies.

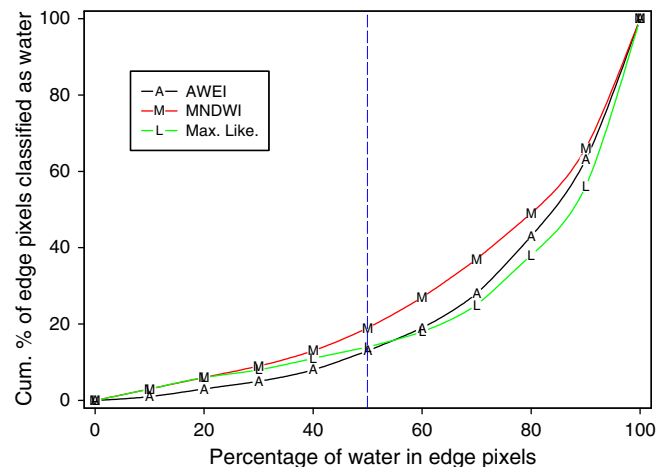


Fig. 5. Cumulative frequency of mixed edge pixels classified as water (average of test sites in Denmark, Switzerland and Ethiopia).

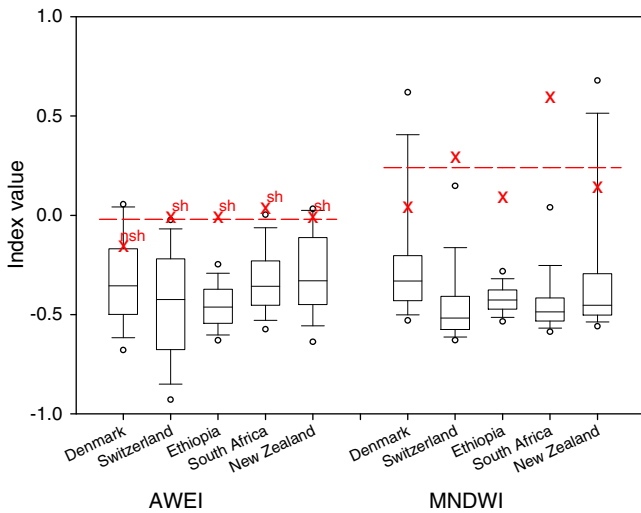


Fig. 6. Threshold variability and distribution of index values for AWEI and MNDWI. Dashed lines show mean optimal threshold of the five test sites, and symbol “x” shows optimal threshold for each site.

In many water indices, the lack of stability of the threshold is a problem (Ji et al., 2009), making it difficult to decide which value should be used in classification trees. The lack of a reasonably stable threshold may make the classification more time-consuming and lead to a subjective choice of threshold which may also affect accuracy. In addition to accuracy improvement, our new index was also shown to have a relatively stable optimal threshold which makes the use of the method even simpler. It should be noted that in our study, images from all test sites were atmospherically corrected applying the FLAASH module in ENVI v.4.8. In classifying images that are calibrated to TOA reflectance, but with no atmospheric corrections, the optimal thresholds may differ slightly from what is observed in this study.

A number of authors contributed to previous research on the improvement of surface water mapping accuracy using remotely sensed data, including those that have emphasized the improvement of general land cover classification accuracies (Aguirre-Gutierrez, Seijmonsbergen, & Duivenvoorden, 2012; Rozenstein & Karnieli, 2011) and surface water mapping in particular (Ji et al., 2009; Sun et al., 2012; Verpoorter et al., 2012; Xu, 2006). In a recent work of Verpoorter et al. (2012), a six-step water extraction method called GeoCover Water Bodies Extraction Method (GWEM) was introduced. In GWEM, the authors proposed a combination of various classification techniques for improvement of accuracy. The same authors identified shadows of cloud and mountains as major sources of accuracy problems and proposed a method where elevation data were used to detect shadows and water surfaces that overlap with shadow were removed from the classification dataset. Our new method which automatically suppresses shadow pixels without the need for other data input or separate shadow detection procedures, may ease surface water mapping, particularly in situations where mapping, monitoring and change detection of surface water resources across multiple scenes or over regional and global scales are required.

Despite a number of surface water mapping and accuracy improvement methods reported in the literature, limited research has been undertaken on accuracy assessment at sub-pixel level. This is particularly important when satellite images such as Landsat are used. Because of the limited spatial resolution of reflective bands of Landsat TM, edge pixels cover relatively large areas which likely consist of a mixture of water and nonwater components. In the use of Landsat TM data for environmental studies where monitoring and detecting changes in

waterline are of interest, the accuracy of classifying mixed edge pixels may become an important issue.

As mentioned in the Results section, when applying the ML classifier to the reservoirs around Addis Ababa, a substantial number of edge pixels that predominantly consist of water were classified as nonwater, thus obviously leading to underestimation of surface water extents. The implication of this could be that even if the water boundary increases by certain distance, thus changing the proportion of water in mixed edge pixels, say from 40% to 60%, the ML method could still classify the pixels as nonwater since it seems that the classifier is sensitive to nonwater components of the mixture. The ability of different classifiers to classify such mixed pixels correctly into water and nonwater classes may vary depending on the spectral bands and algorithms used. The nonwater components of the mixture could be composed of many combinations of different land cover types. So, the reflectance values of mixed pixels can vary considerably, even for pixels where the proportion of water is similar (Ji et al., 2009). The relative improvement in sub-pixel accuracy achieved by AWEI may make it suitable for consistent and reliable estimation of surface water dynamics using Landsat data.

Though the new water extraction index was tested under wide range of environmental conditions and water body types, several variables that were not considered at our test sites are likely to affect the accuracy of water extraction methods. Seasonal and daily variation in the angle of the sun, atmospheric composition, and changes in biophysical and chemical properties of water bodies, such as changes in phytoplankton (Zhang et al., 2010) may influence the reflectance patterns of water bodies. The use of different atmospheric correction methods may also influence thresholds and accuracies. Therefore one may need to consider the importance and type of atmospheric correction applied in the image preprocessing stage in evaluating accuracies of different water extraction methods. AWEI was tested using Landsat TM data only and its use may therefore need to be evaluated on data from other sensors.

In our test cases, we did not consider the influence of seasonal variation in appearances of water bodies. Therefore, the robustness of the new method also needs to be tested in different seasons. In addition to the five test sites examined in details, we included three additional sites in Appendix A (Figs. A1–A3). Nevertheless, more sites may need to be included for a thorough evaluation of the performance of the index.

6. Conclusion

The main purpose of this study was to devise a method that improves water extraction accuracy by increasing spectral separability between water and nonwater surfaces, particularly in areas with shadows and urban backgrounds that are often major causes of low classification accuracy. Using Landsat 5 TM data, we introduced a new automated water extraction method (AWEI) and compared its per-pixel and sub-pixel accuracy and threshold stability with that of the MNDWI and ML classifiers. AWEI significantly improved accuracy in areas where shadow and other dark surfaces were the main sources of classification errors.

A sub-pixel analysis of errors at the edges of water bodies revealed that the AWEI classifier was relatively more accurate in classifying edge pixels compared to the MNDWI and ML classification methods. Besides, the optimal threshold of AWEI was shown to be less variable with images of different locations and times compared to that of MNDWI. Therefore, AWEI is proposed as an alternative and improved water index, especially in extracting water information from areas where noisy results are expected because of the presence of shadows and built-up surfaces. This new method would also be suitable for surface water change detection studies since it classifies edge pixels with high accuracy and with a stable threshold.

Appendix A

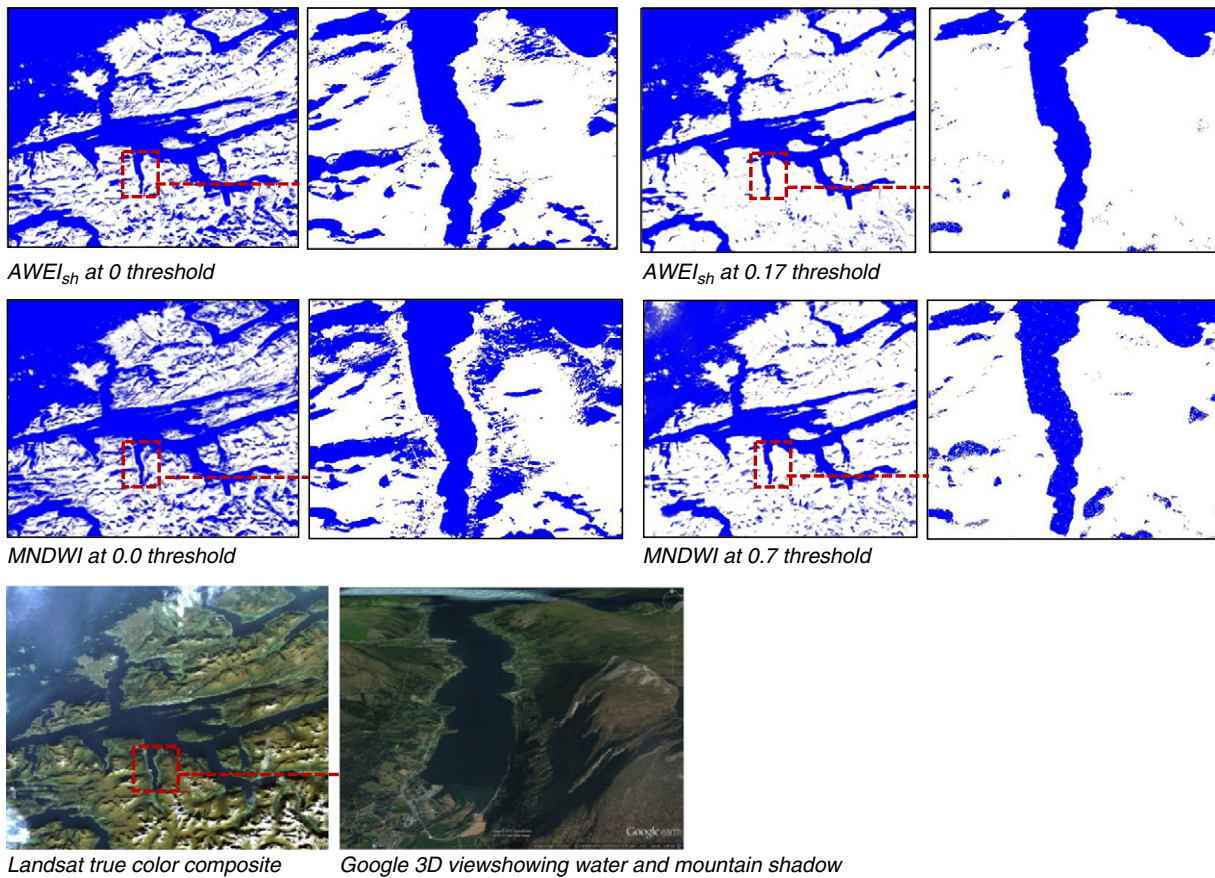


Fig. A1. Water extraction images applying AWEI_{sh} (top row) and MNDWI (middle row) at test site in Norway using Landsat 5 TM acquired on Aug 13, 2011 (2382 by 2382 pixels, top-left corner coordinate in UTM: 6,989,655 N, 371,295 E).

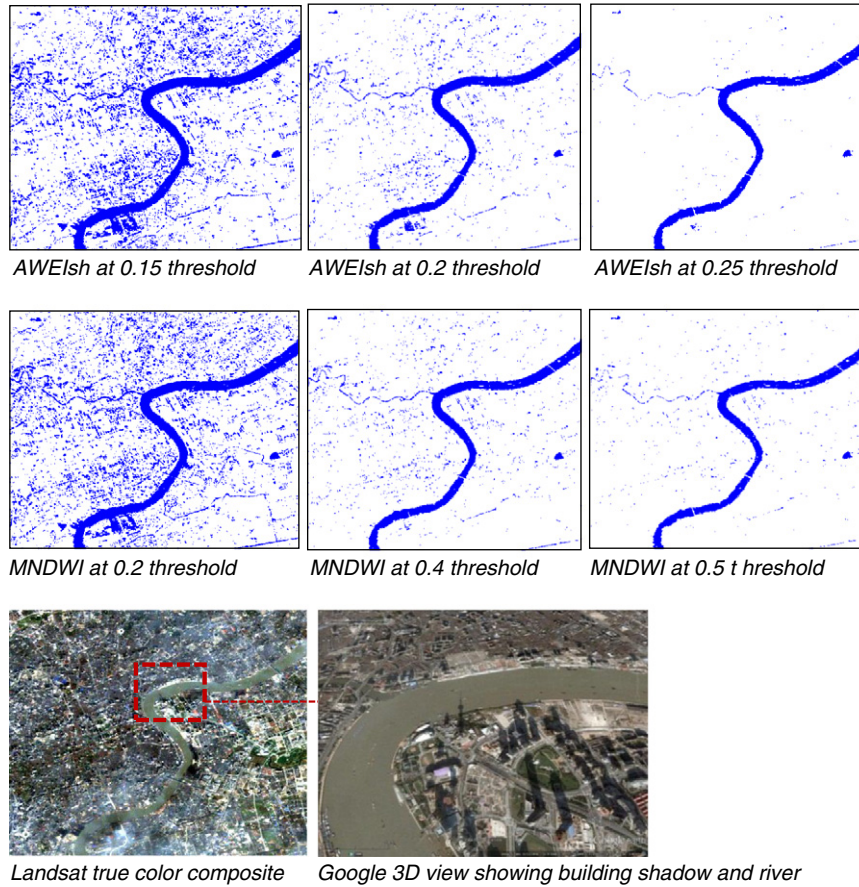


Fig. A2. Water extraction images applying $AWEI_{sh}$ (top row) and MNDWI (middle row) at test site in China Shanghai using Landsat ETM+ acquired on Nov 27, 2002 (400 by 400 pixels, top-left corner coordinate UTM: 3,461,925 N, 350,415 E).

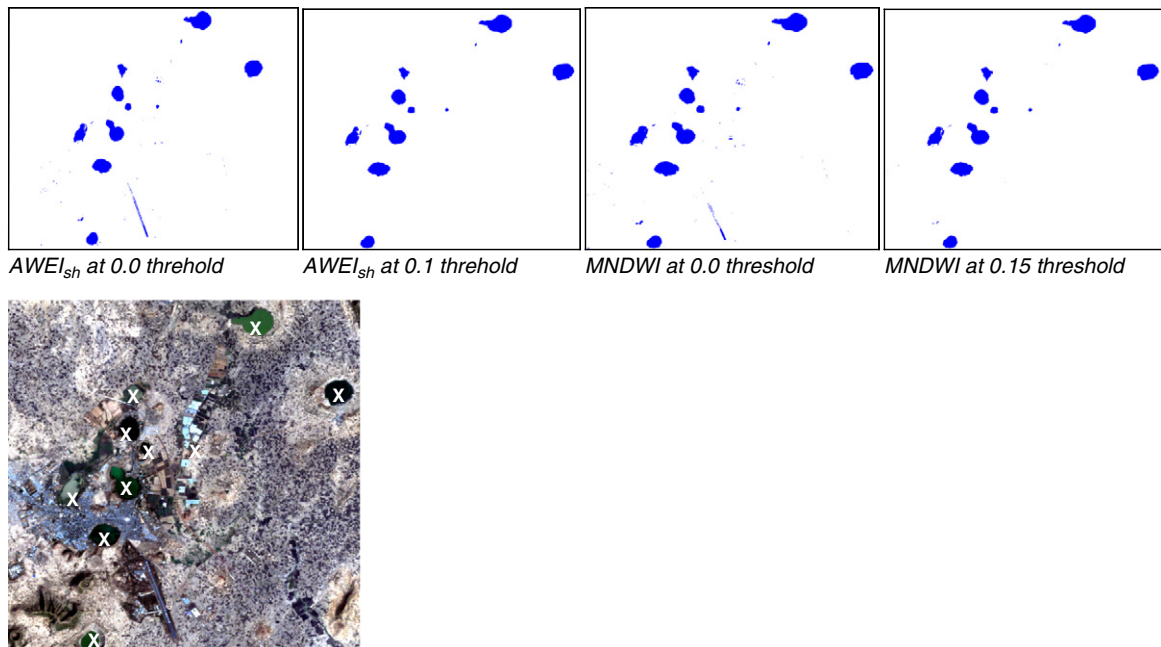


Fig. A3. Water extraction images applying $AWEI_{sh}$ (top row) and MNDWI (middle row) at test site in Bishftu Ethiopia using Landsat ETM+ acquired on Nov 27, 2002 (400 by 400 pixels, top-left corner coordinate UTM: 3,461,925 N, 350,415 E). Location of actual water bodies is shown by “X” mark on true color composite of the Landsat ETM+ image (bottom image).

Table A1
Summary of accuracy assessments at the five main test sites showing various accuracy measures.

Test site	Classification method	Threshold	Land cover class	User accu.	Produc accu.	Kappa	Comm. error %	Omi. error %	Total error %
Denmark	^a AWEI _{hsh}	0.000	Water	97.08	91.43	0.93	2.92	8.57	11.49
			Nonwater	98.57	99.54		1.43	0.46	1.89
		−0.2	Water	96.35	92.89	0.94	3.65	7.11	10.77
			Nonwater	98.81	99.41		1.19	0.59	1.79
		−0.15	Water	98.30	92.58	0.95	1.70	7.42	9.12
			Nonwater	98.75	99.72		1.25	0.28	1.53
	MNDWI	0.00	Water	95.13	91.04	0.92	4.87	8.96	13.82
			Nonwater	98.50	99.22		1.50	0.78	2.28
		0.05	Water	97.10	89.89	0.92	2.90	10.11	13.02
			Nonwater	98.32	99.55		1.68	0.45	2.14
		0.1	Water	98.05	88.65	0.92	1.95	11.35	13.31
			Nonwater	98.12	99.70		1.88	0.30	2.18
	MaxLike	–	Water	96.85	84.61	0.89	3.15	15.39	18.53
	Nonwater	97.46	99.54	2.54	0.46		3.00		
Switzerland	AWEI _{sh}	−0.050	Water	52.89	96.77	0.66	47.1	3.2	50.3
			Nonwater	99.84	95.81		0.2	4.2	4.4
		0.100	Water	99.34	76.61	0.86	0.7	23.4	24.1
			Nonwater	98.88	99.98		1.1	0.0	1.1
		0.000	Water	99.01	90.96	0.95	1.0	9.0	10.0
			Nonwater	99.56	99.96		0.4	0.0	0.5
	MNDWI	−0.005	Water	99.34	76.61	0.94	0.7	23.4	24.1
			Nonwater	99.84	95.81		0.2	4.2	4.4
		0.100	Water	73.92	95.64	0.82	26.1	4.4	30.4
			Nonwater	99.79	98.36		0.2	1.6	1.9
		0.300	Water	87.99	91.92	0.89	12.0	8.1	20.1
			Nonwater	99.61	99.39		0.4	0.6	1.0
	0.500	Water	96.76	78.95	0.86	3.2	21.1	24.3	
		Nonwater	98.99	99.87		1.0	0.1	1.1	
MaxLike	–	Water	74.46	92.08	0.81	25.5	7.9	33.5	
Nonwater	99.61	98.47	0.4	1.5		1.9			
Ethiopia	AWEI _{sh}	−0.050	Water	95.47	98.85	0.95	4.53	1.15	5.68
			Nonwater	100.00	99.97		0.00	0.03	0.04
		0.000	Water	95.47	98.85	0.97	4.53	1.15	5.68
			Nonwater	100.00	99.98		0.00	0.02	0.02
		0.100	Water	96.60	91.48	0.94	3.40	8.52	11.92
			Nonwater	99.97	99.99		0.03	0.01	0.05
	MNDWI	0.000	Water	92.57	96.66	0.95	7.43	3.34	10.77
			Nonwater	99.99	99.97		0.01	0.03	0.04
		0.100	Water	95.01	95.39	0.95	4.99	4.61	9.60
			Nonwater	99.98	99.98		0.02	0.02	0.04
		0.150	Water	97.53	92.66	0.95	2.47	7.34	9.81
			Nonwater	99.97	99.99		0.03	0.01	0.04
	MaxLike	–	Water	99.71	86.96	0.93	0.29	13.04	13.33
	Nonwater	99.95	100.00	0.05	0.00		0.05		
S. Africa	AWEI _{sh}	0.020	Water	83.23	98.86	0.90	16.77	1.14	17.91
			Nonwater	99.97	99.50		0.03	0.50	0.53
		0.045	Water	98.32	98.30	0.98	1.68	1.70	3.38
			Nonwater	99.96	99.96		0.04	0.04	0.09
		0.060	Water	98.43	97.51	0.98	1.57	2.49	4.06
			Nonwater	99.94	99.96		0.06	0.04	0.10
	MNDWI	0.300	Water	70.54	97.67	0.81	29.46	2.33	31.79
			Nonwater	99.94	98.97		0.06	1.03	1.09
		0.450	Water	89.07	96.37	0.92	10.93	3.63	14.56
			Nonwater	99.91	99.70		0.09	0.30	0.39
		0.600	Water	94.46	93.58	0.94	5.54	6.42	11.96
			Nonwater	99.84	99.86		0.16	0.14	0.30
	MaxLik	–	Water	46.74	97.12	0.62	53.26	2.88	56.14
	Nonwater	99.93	97.21	0.07	2.79		2.87		
N. Zealand	AWEI _{sh}	−0.100	Water	98.74	99.87	0.96	1.26	0.13	1.39
			Nonwater	99.29	93.65		0.71	6.35	7.06
		0.000	Water	99.82	99.56	0.98	0.18	0.44	0.61
			Nonwater	97.85	99.13		2.15	0.87	3.02
		0.100	Water	99.90	99.45	0.98	0.10	0.55	0.65
			Nonwater	97.33	99.51		2.67	0.49	3.17
	MNDWI	0.000	Water	96.93	99.79	0.89	3.07	0.21	3.28
			Nonwater	98.79	84.23		1.21	15.77	16.98
		0.150	Water	97.39	99.44	0.90	2.61	0.56	3.16
			Nonwater	96.91	86.72		3.09	13.28	16.37
		0.200	Water	98.14	98.50	0.90	1.86	1.50	3.35
			Nonwater	92.39	90.71		7.61	9.29	16.89
	MaxLike	–	Water	99.84	99.18	0.97	0.16	0.82	0.98
	Nonwater	96.05	99.22	3.95	0.78		4.73		

^a At this test site, shadow is not a major source of classification noise but built-up surfaces are predominant land cover type. Therefore, the use of AWEI_{hsh} resulted in high accuracy of water extraction (a combined use of both AWEI_{sh} and AWEI_{hsh} did not improve accuracy).

References

- Aguirre-Gutierrez, J., Seijmonsbergen, A.C., & Duivenvoorden, J. F. (2012). Optimizing land cover classification accuracy for change detection, a combined pixel-based and object-based approach in a mountainous area in Mexico. *Applied Geography*, 34, 29–37.
- Alderman, K., Turner, L. R., & Tong, S. L. (2012). Floods and human health: A systematic review. *Environment International*, 47, 37–47.
- Bond, N. R., Lake, P. S., & Arthington, A. H. (2008). The impacts of drought on freshwater ecosystems: An Australian perspective. *Hydrobiologia*, 600, 3–16.
- Butcher, S. S., Charlson, R. J., Orians, G. H., & Wolfe, G. V. (Eds.). (1992). *Global biogeochemical cycles*. London: Academic Press Limited.
- Charoenpanyanet, A., & Chen, X. (2008). Satellite-based modeling of *Anopheles* mosquito densities on heterogeneous land cover in Western Thailand. *The International Archives of the Photogrammetry, Remote Sensing and Spatial Information Sciences*, 37, 159–164.
- Charron, D. F., Thomas, M. K., Waltner-Toews, D., Aramini, J. J., Edge, T., Kent, R. A., et al. (2004). Vulnerability of waterborne diseases to climate change in Canada: A review. *Journal of Toxicology and Environmental Health-Part a-Current Issues*, 67, 1667–1677.
- Congalton, R. G., & Green, K. (2009). *Assessing the accuracy of remotely sensed data: Principles and practices* (2nd ed.). Boca Raton: Lewis Publishers.
- COWI (2010). DD0land2010: Danish National Digital Orthophoto, version 2010. <http://www.geodata-info.dk/Portal/ShowMetadata.aspx?id=d6a57343-c930-4d28-94ce-85b5ca2847dc>
- Dambach, P., Machault, V., Lacaux, J.-P., Vignolles, C., Sié, A., & Sauerborn, R. (2012). Utilization of combined remote sensing techniques to detect environmental variables influencing malaria vector densities in rural West Africa. *International Journal of Health Geographics*, 11.
- Davranche, A., Lefebvre, G., & Poulin, B. (2010). Wetland monitoring using classification trees and SPOT-5 seasonal time series. *Remote Sensing of Environment*, 114, 552–562.
- De Leeuw, J., Jia, H., Yang, L., Liu, X., Schmidt, K., & Skidmore, A. K. (2006). Comparing accuracy assessments to infer superiority of image classification methods. *International Journal of Remote Sensing*, 27, 223–232.
- Dewan, A.M., Islam, M. M., Kumamoto, T., & Nishigaki, M. (2007). Evaluating flood hazard for land-use planning in Greater Dhaka of Bangladesh using remote sensing and GIS techniques. *Water Resources Management*, 21, 1601–1612.
- Duan, Z., & Bastiaanssen, W. G. M. (2013). Estimating water volume variations in lakes and reservoirs from four operational satellite altimetry databases and satellite imagery data. *Remote Sensing of Environment*, 134, 403–416.
- Exelis Visual Information Solutions (2010). *ENVI v. 4.8*. Boulder, Colorado: EXELIS.
- Frey, H., Huggel, C., Paul, F., & Haeblerli, W. (2010). Automated detection of glacier lakes based on remote sensing in view of assessing associated hazard potentials. *Grazer Schriften der Geographie und Raumforschung*, 45, 261–272.
- Gardelle, J., Hiernaux, P., Kergoat, L., & Grippa, M. (2009). Less rain, more water in ponds: A remote sensing study of the dynamics of surface waters from 1950 to present in pastoral Sahel (Gourma region, Mali). *Hydrology and Earth System Sciences Discussions*, 6, 5047–5083.
- Giardino, C., Bresciani, M., Villa, P., & Martinelli, A. (2010). Application of remote sensing in water resource management: The case study of Lake Trasimeno, Italy. *Water Resources Management*, 24, 3885–3899.
- Guttler, F. N., Niculescu, S., & Gohin, F. (2013). Turbidity retrieval and monitoring of Danube Delta waters using multi-sensor optical remote sensing data: An integrated view from the delta plain lakes to the western-northwestern Black Sea coastal zone. *Remote Sensing of Environment*, 132, 86–101.
- Haas, E. M., Bartholomé, E., & Combal, B. (2009). Time series analysis of optical remote sensing data for the mapping of temporary surface water bodies in sub-Saharan western Africa. *Journal of Hydrology*, 370, 52–63.
- He, B., Oki, K., Wang, Y., Oki, T., Yamashiki, Y., Takara, K., et al. (2012). Analysis of stream water quality and estimation of nutrient load with the aid of Quick Bird remote sensing imagery. *Hydrological Sciences Journal/Des Sciences Hydrologiques*, 57, 850–860.
- Hui, F., Xu, B., Huang, H., Yu, Q., & Gong, P. (2008). Modelling spatial-temporal change of Poyang Lake using multitemporal Landsat imagery. *International Journal of Remote Sensing*, 29, 5767–5784.
- Jain, S. K., Saraf, A. K., Goswami, A., & Ahmad, T. (2006). Flood inundation mapping using NOAA AVHRR data. *Water Resources Management*, 20, 949–959.
- Jain, S. K., Singh, R. D., Jain, M. K., & Lohani, A. K. (2005). Delineation of flood-prone areas using remote sensing technique. *Water Resources Management*, 19, 337–347.
- Ji, L., Zhang, L., & Wylie, B. (2009). Analysis of dynamic thresholds for the normalized difference water index. *Photogrammetric Engineering and Remote Sensing*, 75, 1307–1317.
- Jiang, Z., Qi, J., Su, S., Zhang, Z., & Wu, J. (2012). Water body delineation using index composition and HIS transformation. *International Journal of Remote Sensing*, 33, 3402–3421.
- Jimenez-Munoz, J. C., Sobrino, J. A., Mattar, C., & Franch, B. (2010). Atmospheric correction of optical imagery from MODIS and reanalysis atmospheric products. *Remote Sensing of Environment*, 114, 2195–2210.
- Kondo, H., Seo, N., Yasuda, T., Hasizume, M., Koido, Y., Ninomiya, N., et al. (2002). Post-flood-infectious diseases in Mozambique. *Prehospital and Disaster Medicine*, 17, 126–133.
- Lacaux, J. P., Tourre, Y. M., Vignolles, C., Ndione, J. A., & Lafaye, M. (2007). Classification of ponds from high-spatial resolution remote sensing: Application to Rift Valley Fever epidemics in Senegal. *Remote Sensing of Environment*, 106, 66–74.
- Lake, P.S. (2003). Ecological effects of perturbation by drought in flowing waters. *Freshwater Biology*, 48, 1161–1172.
- Li, K. Z., Wu, S. H., Dai, E. F., & Xu, Z. C. (2012). Flood loss analysis and quantitative risk assessment in China. *Natural Hazards*, 63, 737–760.
- Lillesand, T. M., Kiefer, R. W., & Chipman, J. W. (2004). *Remote sensing and image interpretation* (5th ed.): John Wiley & Sons, Inc.
- Lira, J. (2006). Segmentation and morphology of open water bodies from multispectral images. *International Journal of Remote Sensing*, 27, 4015–4038.
- McPeeters, S. K. (1996). The use of Normalized Difference Water Index (NDWI) in the delineation of open water features. *International Journal of Remote Sensing*, 17, 1425–1432.
- Morss, R. E., Wilhelm, O. V., Downton, M. W., & Grunfest, E. (2005). Flood risk, uncertainty, and scientific information for decision making – Lessons from an interdisciplinary project. *Bulletin of the American Meteorological Society*, 86 (1593–+).
- Mucher, C. A., Steinnocher, K. T., Kressler, F. P., & Heunks, C. (2000). Land cover characterization and change detection for environmental monitoring of pan-Europe. *International Journal of Remote Sensing*, 21, 1159–1181.
- NASA (2012). Landsat 7 science data users handbook. *Online*.
- Novoa, S., Chust, G., Sagarminaga, Y., Revilla, M., Borja, A., & Franco, J. (2012). Water quality assessment using satellite-derived chlorophyll-a within the European directives, in the southeastern Bay of Biscay. *Marine Pollution Bulletin*, 64, 739–750.
- Ouma, Y. O., & Tateishi, R. (2006). A water index for rapid mapping of shoreline changes of five East African Rift Valley lakes: An empirical analysis using Landsat TM and ETM+ data. *International Journal of Remote Sensing*, 27, 3153–3181.
- Poulin, B., Davranche, A., & Lefebvre, G. (2010). Ecological assessment of *Phragmites australis* wetlands using multi-season SPOT-5 scenes. *Remote Sensing of Environment*, 114, 1602–1609.
- Prigent, C., Papa, F., Aires, F., Jimenez, C., Rossow, W. B., & Matthews, E. (2012). Changes in land surface water dynamics since the 1990s and relation to population pressure. *Geophysical Research Letters*, 39, L08403.
- Proud, S. R., Fensholt, R., Rasmussen, L. Y., & Sandholt, I. (2011). Rapid response flood detection using the MSG geostationary satellite. *International Journal of Applied Earth Observation and Geoinformation*, 13, 536–544.
- Richards, J. A. (1993). *Remote sensing digital image analysis: An introduction* (2nd ed.). Berlin: Springer-Verlag.
- Rogers, A. S., & Kearney, M. S. (2004). Reducing signature variability in unmixed coastal marsh Thematic Mapper scenes using spectral indices. *International Journal of Remote Sensing*, 25, 2317–2335.
- Rozenstein, O., & Karnieli, A. (2011). Comparison of methods for land-use classification incorporating remote sensing and GIS inputs. *Applied Geography*, 31, 533–544.
- Ryu, J. H., Won, J. S., & Min, K. D. (2002). Waterline extraction from Landsat TM data in a tidal flat – A case study in Gomsu Bay, Korea. *Remote Sensing of Environment*, 83, 442–456.
- Sethre, P. R., Rundquist, B. C., & Todhunter, P. E. (2005). Remote detection of prairie pot-hole ponds in the Devils Lake Basin, North Dakota. *GIScience and Remote Sensing*, 42, 277–296.
- Sheng, Y. W., Shah, C. A., & Smith, L. C. (2008). Automated image registration for hydrologic change detection in the lake-rich Arctic. *IEEE Geoscience and Remote Sensing Letters*, 5, 414–418.
- Sun, F., Sun, W., Chen, J., & Gong, P. (2012). Comparison and improvement of methods for identifying waterbodies in remotely sensed imagery. *International Journal of Remote Sensing*, 33, 6854–6875.
- United States Geological Survey (USGS) (2012). Landsat data archive. *Global Visualization Viewer (GLOVIS)*.
- Verpoorter, C., Kutser, T., & Tranvik, L. (2012). Automated mapping of water bodies using Landsat multispectral data. *Limnology and Oceanography-Methods*, 10, 1037–1050.
- Xu, H. (2006). Modification of normalised difference water index (NDWI) to enhance open water features in remotely sensed imagery. *International Journal of Remote Sensing*, 27, 3025–3033.
- Zhang, Y. L., Feng, L. Q., Li, J. S., Luo, L. C., Yin, Y., Liu, M. L., et al. (2010). Seasonal-spatial variation and remote sensing of phytoplankton absorption in Lake Taihu, a large eutrophic and shallow lake in China. *Journal of Plankton Research*, 32, 1023–1037.